Florence, Italy 12-16 July 2015
ICSV22
The 22nd International Congress on Sound and Vibration

GEOPHYSICAL NOISE INTERFEROMETRY: REPAIRING THE BROKEN MIRROR

Kees Wapenaar, Joost van der Neut, Deyan Draganov
Department of Geoscience and Engineering, Delft University of Technology, Delft, The Netherlands
email: c.p.a.wapenaar@tudelft.nl

Elmer Ruigrok
Department of Earth Sciences, Utrecht University, Utrecht, The Netherlands

Under conditional circumstances, the correlation of noise at two receivers is approximately proportional to the Green's function between these receivers. Hence, the correlation process turns one of the receivers into a virtual source, of which the response is observed by the other receiver. This principle, also known as ambient-noise interferometry, is used by researchers in geophysics, ultrasonics and underwater acoustics to infer information about an unknown object from passive noise measurements. In geophysics, ambient-noise interferometry is used for tomographic velocity inversion when surface waves are dominant, or for high-resolution reflection imaging when a significant amount of body waves is present in the noise field.

The virtual-source response obtained with geophysical noise interferometry is accurate when the medium is lossless and the noise field is equipartitioned. In practice these assumptions are often violated: the medium of interest is often illuminated from one side only, the sources may be irregularly distributed and losses may be significant. For those cases, it is as if the virtual source is viewed in a broken (time-reversal) mirror, which causes blurring of the source. This blurring is quantified by the so-called point-spread function, which, like the correlation function, can be derived from the observed data (that is, without the need to know the actual sources and the medium). The broken mirror can be repaired by deconvolving the correlation function for the point-spread function. As a result, the virtual source is refocused and hence the virtual-source response becomes more reliable.

1. Introduction

In recent years, the methodology of Green's function retrieval by crosscorrelation has led to many applications in seismology (exploration, regional and global), underwater acoustics and ultrasonics. In seismology this methodology is also called "seismic interferometry". One of the explanations for the broad interest lies in the fact that new responses can be obtained from measured data in a very simple way. In passive-data applications, a straightforward crosscorrelation of responses at two receivers approximates the impulse response (Green's function) at one receiver of a virtual source at the position of the other [5, 8]. In controlled-source applications the procedure is similar, except that it involves in addition a summation over the sources [6].

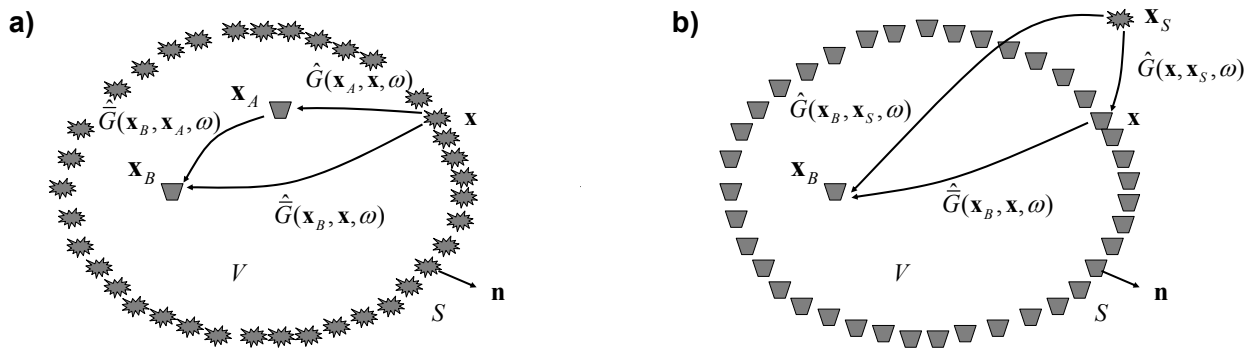

Figure 1: *(a) Configuration for the correlation-type Green's function representation (Eq. 1). The medium in $\mathbb{V}$ is assumed lossless. The rays represent full responses, including primary and multiple scattering due to inhomogeneities inside as well as outside $\mathbb{S}$. (b) Configuration for the convolution-type Green's function representation (Eq. 2). Here the medium does not need to be lossless.*

It has also been recognized that the simple crosscorrelation approach has its limitations. From the various theoretical models it follows that there is a number of underlying assumptions for retrieving the Green's function by crosscorrelation. The most important assumptions are that the medium is lossless and that the waves are equipartitioned. In heuristic terms, the latter condition means that the receivers are illuminated isotropically from all directions, which is for example achieved when the sources are regularly distributed along a closed surface, the sources are mutually uncorrelated (in case of simultaneous recordings) and their power spectra are identical. Despite the fact that in practical situations these conditions are at most only partly fulfilled, the results of seismic interferometry are generally quite robust, but the retrieved amplitudes are unreliable and the results are often blurred by artifacts.

In this tutorial paper, which summarizes earlier work [15], we show how these shortcomings can be overcome by a multidimensional deconvolution process.

2. Green's function representations for seismic interferometry

We briefly review two Green's function representations for seismic interferometry. Consider a volume $\mathbb{V}$ enclosed by a surface $\mathbb{S}$, with outward pointing normal vector $\mathbf{n} = (n_1, n_2, n_3)$. In $\mathbb{V}$ we have an arbitrary inhomogeneous medium with acoustic propagation velocity $c(\mathbf{x})$ and mass density $\rho(\mathbf{x})$ (where $\mathbf{x} = (x_1, x_2, x_3)$ is the Cartesian coordinate vector). We consider two points in $\mathbb{V}$, denoted by coordinate vectors $\mathbf{x}_A$ and $\mathbf{x}_B$, see Fig. 1a. We define the Fourier transform of a time-dependent function $u(t)$ as $\hat{u}(\omega) = \int_{-\infty}^{\infty} \exp(-j\omega t)u(t)\mathrm{d}t$, with j the imaginary unit and ω the angular frequency. Assuming the medium in $\mathbb{V}$ is lossless, the correlation-type representation for the acoustic Green's function between $\mathbf{x}_A$ and $\mathbf{x}_B$ in $\mathbb{V}$ reads [14]

$$\hat{\bar{G}}(\mathbf{x}_B,\mathbf{x}_A,\omega) + \hat{G}^*(\mathbf{x}_B,\mathbf{x}_A,\omega) = - \oint_{\mathbb{S}} \frac{1}{j\omega\rho(\mathbf{x})} \Big(\partial_i \hat{\bar{G}}(\mathbf{x}_B,\mathbf{x},\omega)\hat{G}^*(\mathbf{x}_A,\mathbf{x},\omega) - \hat{\bar{G}}(\mathbf{x}_B,\mathbf{x},\omega)\partial_i \hat{G}^*(\mathbf{x}_A,\mathbf{x},\omega) \Big) n_i \,\mathrm{d}\mathbf{x} \quad (1)$$

(Einstein's summation convention applies to repeated lower case Latin subscripts). This representation is a basic expression for seismic interferometry (or Green's function retrieval) by crosscorrelation in open systems. The superscript asterisk * denotes complex conjugation, hence, the products on the right-hand side correspond to crosscorrelations in the time domain of observations at two receivers at $\mathbf{x}_A$ and $\mathbf{x}_B$. The notation $\hat{\bar{G}}$ is introduced to denote a reference state with possibly different boundary conditions at $\mathbb{S}$ and/or different medium parameters outside $\mathbb{S}$ (but in $\mathbb{V}$ the medium parameters for

$\hat{\bar{G}}$ are the same as those for $\hat{G}$). The bar is usually omitted because $\hat{G}$ and $\hat{\bar{G}}$ are usually defined in the same medium throughout space. The Green's functions on the left-hand side are the Fourier transforms of the response of a source at $\mathbf{x}_A$ observed at $\mathbf{x}_B$ and its time-reversed version. The representation formulated by Eq. (1) is exact, hence, it accounts not only for the direct wave, but also for primary and multiply scattered waves.

Next, we consider a convolution-type representation for the Green's function. We slightly modify the configuration by taking $\mathbf{x}_A$ outside $\mathbb{S}$ and renaming it $\mathbf{x}_S$, see Fig. 1b. For this configuration the convolution-type representation is given by

$$\hat{G}(\mathbf{x}_B,\mathbf{x}_S,\omega) = -\oint_{\mathbb{S}} \frac{1}{j\omega\rho(\mathbf{x})}\Big(\partial_i\hat{\bar{G}}(\mathbf{x}_B,\mathbf{x},\omega)\hat{G}(\mathbf{x},\mathbf{x}_S,\omega) - \hat{\bar{G}}(\mathbf{x}_B,\mathbf{x},\omega)\partial_i\hat{G}(\mathbf{x},\mathbf{x}_S,\omega)\Big)n_i\,\mathrm{d}\mathbf{x}. \tag{2}$$

Due to the absence of complex-conjugation signs, the products on the right-hand side correspond to crossconvolutions in the time domain. An important difference with the correlation-type representation is that this representation remains valid in media with losses. Again, the bar in $\hat{\bar{G}}$ refers to a reference state with possibly different boundary conditions at $\mathbb{S}$ and/or different medium parameters outside $\mathbb{S}$. We will use Eq. (2) as the starting point for interferometry by deconvolution in open systems. By considering $\hat{\bar{G}}(\mathbf{x}_B,\mathbf{x},\omega)$ under the integral as the unknown quantity, Eq. (2) needs to be resolved by multidimensional deconvolution (MDD).

3. Basic aspects of interferometry by multidimensional deconvolution

3.1 Simplification of the integral

The right-hand side of Eq. (2) contains a combination of two convolution products. Here we will combine these two terms into a single term. The Green's function $\hat{\bar{G}}(\mathbf{x}_B,\mathbf{x},\omega)$ under the integral is the unknown that we want to resolve by MDD. The Green's function $\hat{G}(\mathbf{x}_B,\mathbf{x}_S,\omega)$ on the left-hand side and $\hat{G}(\mathbf{x},\mathbf{x}_S,\omega)$ under the integral are related to the observations. Hence, $\hat{G}$ is defined in the actual medium inside as well as outside $\mathbb{S}$, but for $\hat{\bar{G}}$ we are free to choose convenient boundary conditions at $\mathbb{S}$. In the following we let $\mathbb{S}$ be an absorbing boundary for $\hat{\bar{G}}(\mathbf{x}_B,\mathbf{x},\omega)$, so that its reciprocal $\hat{\bar{G}}(\mathbf{x},\mathbf{x}_B,\omega)$ is outward propagating at $\mathbb{S}$. Furthermore, we write $\hat{G}(\mathbf{x},\mathbf{x}_S,\omega)$ as the superposition of an inward- and outward-propagating part at $\mathbf{x}$ on $\mathbb{S}$, according to $\hat{G}(\mathbf{x},\mathbf{x}_S,\omega) = \hat{G}^{\mathrm{in}}(\mathbf{x},\mathbf{x}_S,\omega) + \hat{G}^{\mathrm{out}}(\mathbf{x},\mathbf{x}_S,\omega)$. Using high-frequency approximations for the derivatives, it follows that Eq. (2) simplifies to [14]

$$\hat{G}(\mathbf{x}_B,\mathbf{x}_S,\omega) = \oint_{\mathbb{S}_{\mathrm{rec}}} \hat{\bar{G}}_{\mathrm{d}}(\mathbf{x}_B,\mathbf{x},\omega)\hat{G}^{\mathrm{in}}(\mathbf{x},\mathbf{x}_S,\omega)\,\mathrm{d}\mathbf{x}, \tag{3}$$

with the dipole Green's function $\hat{\bar{G}}_{\mathrm{d}}$ defined as

$$\hat{\bar{G}}_{\mathrm{d}}(\mathbf{x}_B,\mathbf{x},\omega) = \frac{-2}{j\omega\rho}\big(n_i\partial_i\hat{\bar{G}}(\mathbf{x}_B,\mathbf{x},\omega)\big). \tag{4}$$

We added a subscript 'rec' in $\mathbb{S}_{\mathrm{rec}}$ in Eq. (3) to denote that the integration surface contains the receivers of the Green's function $\hat{G}^{\mathrm{in}}$. In most practical situations, receivers are not available on a closed boundary, so the integration in Eq. (3) is necessarily restricted to an open receiver boundary $\mathbb{S}_{\mathrm{rec}}$. As long as the source position $\mathbf{x}_S$ is located at the appropriate side of $\mathbb{S}_{\mathrm{rec}}$ (i.e., outside $\mathbb{V}$), it suffices to take the integral over an open receiver boundary. Hence, in the following we replace the closed boundary integral by an open boundary integral. In the time domain, Eq. (3) thus becomes

$$G(\mathbf{x}_B,\mathbf{x}_S,t) = \int_{\mathbb{S}_{\mathrm{rec}}} \bar{G}_{\mathrm{d}}(\mathbf{x}_B,\mathbf{x},t) * G^{\mathrm{in}}(\mathbf{x},\mathbf{x}_S,t)\,\mathrm{d}\mathbf{x}, \tag{5}$$

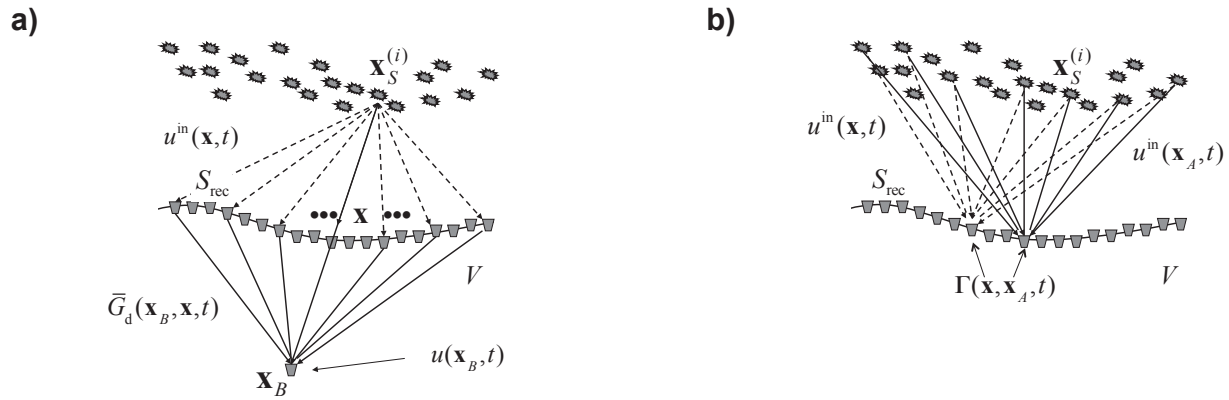

Figure 2: *(a) Illustration of the convolutional model (Eq. 8), underlying interferometry by MDD. The inward-propagating field $u^{\text{in}}(\mathbf{x},t)$ is convolved with $\bar{G}_{\text{d}}(\mathbf{x}_B,\mathbf{x},t)$ and the results for all receivers $\mathbf{x}$ are integrated along the receiver boundary $\mathbb{S}_{\text{rec}}$, giving the response $u(\mathbf{x}_B,t)$. (b) Illustration of the point-spread function $\Gamma(\mathbf{x},\mathbf{x}_A,t)$ (Eq. 11), defined as the crosscorrelation of the inward-propagating fields at $\mathbf{x}$ and $\mathbf{x}_A$ on $\mathbb{S}_{\text{rec}}$. In the ideal case, it is proportional to a band-limited delta function on $\mathbb{S}_{\text{rec}}$, but in practice there are many factors that make it different from a delta function.*

where the in-line asterisk $*$ denotes temporal convolution. Unlike the correlation-type representation (Eq. 1), which holds under the condition that $\mathbb{S}$ is a closed surface, the convolution-type representation of Eq. (5) holds as long as the open surface $\mathbb{S}_{\text{rec}}$ is sufficiently smooth and $\mathbf{x}_B$ and $\mathbf{x}_S$ lie on opposite sides of $\mathbb{S}_{\text{rec}}$. Moreover, whereas Eq. (1) only holds for lossless media, Eq. (5) also holds in media with losses. Equation (5) is an implicit representation of the convolution type for $\bar{G}_{\text{d}}(\mathbf{x}_B,\mathbf{x},t)$. If it were a single equation, the inverse problem would be ill-posed. However, Eq. (5) holds for each source position $\mathbf{x}_S$ (outside $\mathbb{V}$), which we will denote from hereon by $\mathbf{x}_S^{(i)}$, where i denotes the source number. Solving the ensemble of equations (for many $\mathbf{x}_S^{(i)}$) for $\bar{G}_{\text{d}}(\mathbf{x}_B,\mathbf{x},t)$ involves MDD.

3.2 Modifying the representation for noise sources

Suppose that the sources at $\mathbf{x}_S^{(i)}$ are noise sources, with noise functions $N^{(i)}(t)$. When the noise sources act simultaneously, the responses at $\mathbf{x}$ and $\mathbf{x}_B$ can be written as

$$u^{\text{in}}(\mathbf{x},t) = \sum_i G^{\text{in}}(\mathbf{x},\mathbf{x}_S^{(i)},t) * N^{(i)}(t), \tag{6}$$

$$u(\mathbf{x}_B,t) = \sum_i G(\mathbf{x}_B,\mathbf{x}_S^{(i)},t) * N^{(i)}(t). \tag{7}$$

Combining these expressions with Eq. (5), we obtain

$$u(\mathbf{x}_B,t) = \int_{\mathbb{S}_{\text{rec}}} \bar{G}_{\text{d}}(\mathbf{x}_B,\mathbf{x},t) * u^{\text{in}}(\mathbf{x},t)\,\text{d}\mathbf{x}. \tag{8}$$

This expression is illustrated in Fig. 2a. Next, we crosscorrelate both sides of this equation with $u^{\text{in}}(\mathbf{x}_A,t)$, which is defined by Eq. (6) with $\mathbf{x}$ replaced by $\mathbf{x}_A$ (also situated on $\mathbb{S}_{\text{rec}}$). Correlation with $u^{\text{in}}(\mathbf{x}_A,t)$ will be denoted as convolution with $u^{\text{in}}(\mathbf{x}_A,-t)$. This gives

$$C(\mathbf{x}_B,\mathbf{x}_A,t) = \int_{\mathbb{S}_{\text{rec}}} \bar{G}_{\text{d}}(\mathbf{x}_B,\mathbf{x},t) * \Gamma(\mathbf{x},\mathbf{x}_A,t)\ \text{d}\mathbf{x}, \tag{9}$$

with

$$C(\mathbf{x}_B,\mathbf{x}_A,t) = \langle u(\mathbf{x}_B,t) * u^{\text{in}}(\mathbf{x}_A,-t)\rangle, \tag{10}$$

$$\Gamma(\mathbf{x},\mathbf{x}_A,t) = \langle u^{\text{in}}(\mathbf{x},t) * u^{\text{in}}(\mathbf{x}_A,-t)\rangle, \tag{11}$$

where $\langle\cdot\rangle$ denotes averaging. Here $C(\mathbf{x}_B, \mathbf{x}_A, t)$ is the correlation function, as commonly used in ambient-noise interferometry (except for the superscript 'in' in Eq. (10)), and which under certain conditions converges to the Green's function. Equation (9) formulates more precisely the relation between the correlation function and the Green's function. It shows that the correlation function $C(\mathbf{x}_B, \mathbf{x}_A, t)$ is proportional to the sought Green's function $\bar{G}_\mathrm{d}(\mathbf{x}_B, \mathbf{x}, t)$, with its source smeared in space and time by $\Gamma(\mathbf{x}, \mathbf{x}_A, t)$. We call $\Gamma(\mathbf{x}, \mathbf{x}_A, t)$ therefore the interferometric point-spread function (or plainly the point-spread function). $\Gamma(\mathbf{x}, \mathbf{x}_A, t)$, as defined in Eq. (11), is the crosscorrelation of the inward-propagating noise fields at $\mathbf{x}$ and $\mathbf{x}_A$ [11], see Fig. 2b.

If the medium between the source and receiver boundaries were homogeneous and lossless and if the sources would be regularly distributed, mutually uncorrelated noise sources with equal auto-correlation functions $S(t)$ along a large planar boundary (in other words, if we would have a perfect time-reversal mirror), the point-spread function would approach a temporally and spatially band-limited delta function. Hence, for this situation Eq. (9) merely states that the correlation function $C(\mathbf{x}_B, \mathbf{x}_A, t)$ is proportional to the response of a temporally and spatially band-limited source. In practice, there are many factors that make the point-spread function $\Gamma(\mathbf{x}, \mathbf{x}_A, t)$ deviate from a band-limited delta function. Among these factors are medium inhomogeneities, multiple reflections in the illuminating wavefield, intrinsic losses, irregularity of the source distribution, mutual correlation between the different sources, etc. (in other words, the time-reversal mirror is broken). For all those cases, Eq. (9) shows that the point-spread function blurs the source of the Green's function in the spatial directions and generates ghosts in the temporal direction. MDD involves inverting Eq. (9), see section 3.3. Ideally, this removes the distorting effects of the point-spread function $\Gamma(\mathbf{x}, \mathbf{x}_A, t)$ from the correlation function $C(\mathbf{x}_B, \mathbf{x}_A, t)$ and yields an improved estimate of the Green's function $\bar{G}_\mathrm{d}(\mathbf{x}_B, \mathbf{x}, t)$ (in other words, this repairs the broken time-reversal mirror).

3.3 Repairing the broken time-reversal mirror

Interferometry by MDD (i.e., repairing the broken mirror) essentially involves inversion of Eq. (9). In general, the existence of the inverse of the point-spread function is not guaranteed. Recall from Eq. (11) that the point-spread function implicitly involves a summation over source positions. To evaluate this function, the source positions do not need to be known, the source distribution does not need to be regular, and the sources do not need to be completely uncorrelated, but clearly the well-posedness of its inverse depends on the number of available sources, the total source aperture and the source bandwidth. In practical situations, a spectral analysis of the point-spread function helps to assess for which spatial and temporal frequencies the inversion can be carried out [12].

For the actual inversion of Eq. (9) we transform this equation to the frequency domain and replace the integration along the receivers by a summation, according to

$$\hat{C}(\mathbf{x}_B, \mathbf{x}_A^{(l)}, \omega) = \sum_k \hat{\bar{G}}_\mathrm{d}(\mathbf{x}_B, \mathbf{x}^{(k)}, \omega)\hat{\Gamma}(\mathbf{x}^{(k)}, \mathbf{x}_A^{(l)}, \omega), \tag{12}$$

for all $\mathbf{x}_A^{(l)}$ on the receiver surface $\mathbb{S}_\mathrm{rec}$. Note that this discretization assumes a regular sampling of the receiver coordinate $\mathbf{x}^{(k)}$. This is a less severe restriction than that for discretizing a source integral (like in correlation interferometry) because the receivers are often well sampled and their positions are usually known. In case of irregular receiver sampling, a regularization procedure [3] could be applied prior to inverting Eq. (12). Equation (12) can be solved for $\hat{\bar{G}}_\mathrm{d}(\mathbf{x}_B, \mathbf{x}^{(k)}, \omega)$ for each frequency component separately. In practice this is done by a stabilized matrix inversion per frequency component, while taking care of the limitations discussed above. Transforming the end-result back to the time domain gives a band-limited estimate of $\bar{G}_\mathrm{d}(\mathbf{x}_B, \mathbf{x}^{(k)}, t)$, which completes the MDD process.

It is beyond the scope of this paper to discuss the numerical aspects of the matrix inversion. The inversion is similar to that as applied in the context of model-based inverse seismic wavefield extrapolation [2, 13] or data-driven source imaging by time-reversal and inverse filtering [9].

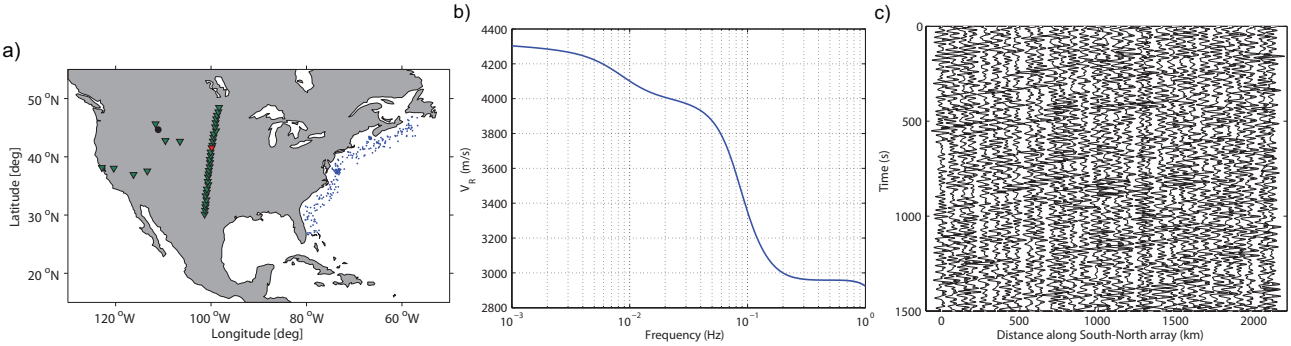

Figure 3: *Model for passive surface-wave interferometry. (a) Map of USA, with USArray stations (green triangles), storm-related microseismic sources (blue dots), and a scatterer (black dot). (b) Rayleigh-wave dispersion curve (fundamental mode), based on the PREM model. (c) Modeled Rayleigh-wave response along South-North array in central USA.*

4. Example: Passive surface-wave interferometry

One of the most widely used applications of geophysical ambient-noise interferometry is the retrieval of seismic surface waves between seismometers from ambient noise [7, 1]. In agreement with the current practice of surface-wave interferometry, in the following numerical example we consider fundamental Rayleigh-wave modes only (but higher order modes can be taken into account as well [10]). The fundamental modes can be treated as the solution of a scalar 2D wave equation with the propagation velocity being the dispersive Rayleigh wave velocity of the layered medium. Hence, for interferometry we can make use of the 2D version of the scalar Green's function representations, discussed in the theory sections. The basic configuration is shown in Fig. 2a. For the current purpose this figure should be seen as a plan view. Consider Fig. 3a, which shows a map of the USA, 38 receiver stations of the USArray (green triangles) and 242 sources along the East coast (blue dots), for example representing storm-related microseismic sources. Moreover, the black dot denotes a strong scatterer, representing the Yellowstone plume. Assuming a layered medium, we compute the dispersion curve of the fundamental mode of the Rayleigh-wave for the upper 300 km of the so-called PREM model [4]. The dispersion curve is shown in Fig. 3b. We define the sources as simultaneously acting uncorrelated noise sources, with a central frequency of 0.04 Hz. Using the computed dispersion curve, we model the surface-wave response of the distribution of noise sources at all indicated receivers. Fig. 3c shows 1500 s of the response along the indicated South-North array in central USA (the total duration of the modeled noise responses is approximately two days).

Our aim is to turn one of the receivers of the South-North array (the one indicated by the red triangle) into a virtual source and to retrieve the response of this virtual source at the irregular receiver stations in the Western USA. Following the crosscorrelation method, we take the noise response at the red receiver and crosscorrelate it with each of the responses at the receivers in the Western USA, i.e., we evaluate $\langle u(\mathbf{x}_B, t) * u(\mathbf{x}_A, -t)\rangle$, with $\mathbf{x}_A$ fixed at the red receiver and $\mathbf{x}_B$ variable. The result is shown in Fig. 4a by the red traces. For comparison, the black traces in this figure represent the directly modeled surface-wave response of a source at the position of the red receiver, using a source function $S(t)$ equal to the average autocorrelation of the noise. There is a pronounced mismatch between the red and black waveforms, as a result of the irregularity of the source distribution (the broken mirror). Overall, the amplitudes of the direct wave are estimated too high, whereas the amplitudes of the scattered event are underestimated.

For the MDD approach, we need to invert Eq. (9), with the correlation and point-spread functions defined in Eqs. (10) and (11), respectively. These expressions contain the inward propagating waves at $\mathbf{x}$ and $\mathbf{x}_A$ on $\mathbb{S}_{\rm rec}$ (which corresponds with the South-North array). Because we consider noise responses we cannot separate the inward propagating waves $u^{\rm in}$ from the outward propagat-

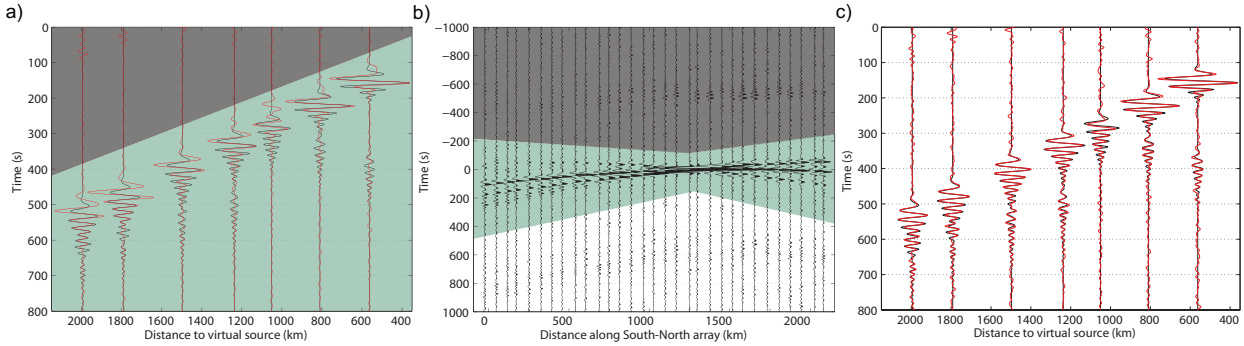

Figure 4: *Passive surface-wave interferometry. (a) Crosscorrelation result (red) compared with directly modeled response (black). The virtual source is indicated by the red receiver in Fig. 3a. The traces correspond to the irregular receiver stations in the Western USA in Fig. 3a. (b) Green-shaded area: approximation of the point-spread function along the South-North array. (c) MDD result (red) compared with directly modeled response (black).*

ing waves u^{out} by time-windowing the observed field u. However, time-windowing can be applied to the correlation function. Recall that Fig. 4a represents the correlation of full wave fields, i.e., $\langle u(\mathbf{x}_B,t) * u(\mathbf{x}_A,-t)\rangle$. From this, we extract $\langle u(\mathbf{x}_B,t) * u^{\text{in}}(\mathbf{x}_A,-t)\rangle$ by removing the events in the gray-shaded area as well as all events at negative time (not shown in Fig. 4a), which together represent $\langle u(\mathbf{x}_B,t) * u^{\text{out}}(\mathbf{x}_A,-t)\rangle$. Hence, we retain only the green-shaded area in Fig. 4a, representing $C(\mathbf{x}_B,\mathbf{x}_A,t) = \langle u(\mathbf{x}_B,t) * u^{\text{in}}(\mathbf{x}_A,-t)\rangle$. To obtain the point-spread function, we first evaluate $\langle u(\mathbf{x},t) * u(\mathbf{x}_A,-t)\rangle$, with $\mathbf{x}_A$ again fixed at the red receiver and $\mathbf{x}$ variable along the South-North array, see Fig. 4b. We remove the events in the white area, representing $\langle u^{\text{out}}(\mathbf{x},t) * u^{\text{in}}(\mathbf{x}_A,-t)\rangle$, and those in the gray-shaded area, representing $\langle u^{\text{in}}(\mathbf{x},t) * u^{\text{out}}(\mathbf{x}_A,-t)\rangle$. We retain the green-shaded area, representing $\langle u^{\text{in}}(\mathbf{x},t) * u^{\text{in}}(\mathbf{x}_A,-t)\rangle + \langle u^{\text{out}}(\mathbf{x},t) * u^{\text{out}}(\mathbf{x}_A,-t)\rangle$. Assuming the outward propagating field is relatively small, we may thus approximate the events in the green-shaded area in Fig. 4b by $\Gamma(\mathbf{x},\mathbf{x}_A,t) = \langle u^{\text{in}}(\mathbf{x},t) * u^{\text{in}}(\mathbf{x}_A,-t)\rangle$. We are now ready to apply MDD (i.e., repairing the broken mirror), which involves inversion of Eq. (9), i.e., removing the effect of the point-spread function (the green-shaded area in Fig. 4b) from the correlation function (the green-shaded area in Fig. 4a). The result is shown by the red traces in Fig. 4c, for display purposes convolved with $S(t)$. Note that the wave forms of the direct wave as well as those of the scattered wave match the directly modeled wave forms (the black traces) much better than in Fig. 4a.

5. Discussion and conclusions

The methodology of seismic interferometry (or Green's function retrieval) by crosscorrelation has a number of attractive properties as well as several limitations. The main attractiveness of the method is that a deterministic medium response can be obtained from passive noise measurements, without the need to know the medium parameters nor the positions of the sources. The fact that this deterministic response is obtained by a straightforward crosscorrelation of two receiver responses has also contributed to the popularity of the method. The main underlying assumptions are that the medium is lossless and that the wave field is equipartitioned, meaning that the net power-flux is zero.

For open systems, the method works well when the receivers that are used in the correlation process are surrounded by a regular distribution of independent transient or uncorrelated noise sources with equal autocorrelation functions. However, in practical situations the method may suffer from irregularities in the source distribution, asymmetric illumination, intrinsic losses, etc.

Fig. 2a illustrates a configuration with an irregular source distribution in a finite region, illuminating the medium from one side only. For this configuration, Eq. (9) shows that the crosscorrelation function $C(\mathbf{x}_B,\mathbf{x}_A,t)$ is a distorted version of the sought Green's function $\bar{G}_{\text{d}}(\mathbf{x}_B,\mathbf{x},t)$. The distor-

tion is quantified by the interferometric point-spread function $\Gamma(\mathbf{x}, \mathbf{x}_A, t)$, which blurs the source of the Green's function in the spatial directions and generates ghosts in the temporal direction [11]. As such, this interferometric point-spread function plays a similar role as the point-spread function in optical, acoustic and seismic imaging systems. When the point-spread function of an imaging system is known, the resolution of an image can be improved by deconvolving for the point-spread function. An interesting aspect is that the interferometric point-spread function can be obtained directly from measured responses, hence, it does not require knowledge of the complex medium nor of the sources. This means that it automatically accounts for the distorting effects of the irregularity of the sources (including variations in their autocorrelation functions), and of the medium inhomogeneities, including multiple scattering.

REFERENCES

1. Bensen, G.D., Ritzwoller, M.H. and Shapiro, N.M. Broadband ambient noise surface wave tomography across the United States. *Journal of Geophysical Research - Solid Earth*, **113**, B05306, (2008).
2. Berkhout, A.J. *Seismic Migration. Imaging of acoustic energy by wave field extrapolation*. Elsevier, Amsterdam, (1982).
3. Duijndam, A.J.W., Schonewille, M.A. and Hindriks, C.O.H. Reconstruction of band-limited signals, irregularly sampled along one spatial direction. *Geophysics*, **64**, 524–538, (1999).
4. Dziewonski, A.M. and Anderson, D.L. Preliminary reference Earth model. *Physics of the Earth and Planetary Interiors*, **25**, 297–356, (1981).
5. Larose, E., Margerin, L., Derode, A., van Tiggelen, B., Campillo, M., Shapiro, N., Paul, A., Stehly, L., and Tanter, M. Correlation of random wave fields: An interdisciplinary review. *Geophysics*, **71** (4), SI11–SI21, (2006).
6. Schuster, G.T. *Seismic interferometry*. Cambridge University Press, (2009).
7. Shapiro, N.M., Campillo, M., Stehly, L. and Ritzwoller, M.H. High-resolution surface-wave tomography from ambient seismic noise. *Science*, **307**, 1615–1618, (2005).
8. Snieder, R., Miyazawa, M., Slob, E., Vasconcelos, I. and Wapenaar, K. A comparison of strategies for seismic interferometry. *Surveys in Geophysics*, **30**, 503–523, (2009).
9. Tanter, M., Thomas, J.L. and Fink, M. Time-reversal and the inverse filter. *Journal of the Acoustical Society of America*, **108** (1), 223–234, (2000).
10. Van Dalen, K.N., Wapenaar, K. and Halliday, D.F. Surface wave retrieval in layered media using seismic interferometry by multidimensional deconvolution. *Geophysical Journal International*, **196**, 230–242, (2014).
11. Van der Neut, J., Ruigrok, E., Draganov, D. and Wapenaar, K. Retrieving the earth's reflection response by multi-dimensional deconvolution of ambient seismic noise. *EAGE, Extended Abstracts*, P406, (2010).
12. Van der Neut, J., Thorbecke, J., Mehta, K., Slob, E. and Wapenaar, K. Controlled-source interferometric redatuming by crosscorrelation and multidimensional deconvolution in elastic media. *Geophysics*, **76** (4), SA63–SA76, (2011).
13. Wapenaar, C.P.A. and Berkhout, A.J. *Elastic wave field extrapolation*. Elsevier, Amsterdam, (1989).
14. Wapenaar, K. and Fokkema, J. Green's function representations for seismic interferometry. *Geophysics*, **71** (4), SI33–SI46, (2006).
15. Wapenaar, K., van der Neut, J., Ruigrok, E., Draganov, D., Hunziker, J., Slob, E., Thorbecke, J., and Snieder, R. Seismic interferometry by crosscorrelation and by multidimensional deconvolution: a systematic comparison. *Geophysical Journal International*, **185**, 1335–1364, (2011).